PROCEEDINGS OF SCIENCE

First observation of tWZ production

Alberto Belvedere[1,*]

Deutsches Elektronen-Synchrotron (DESY),
Notkestrasse 85, Hamburg, Germany

E-mail: alberto.belvedere@cern.ch

We present the first observation of single top quark production in association with a W and a Z boson in proton-proton collisions using 13 and 13.6 TeV data recorded with the CMS detector corresponding to integrated luminosities of 138 and 61.9 fb^{-1}, respectively. Events are selected if they contain three or four charged leptons, which can be electrons or muons. State-of-the-art machine learning algorithms and sophisticated reconstruction methods result in an unprecedented sensitivity to tWZ production. We report the first observation of this rare process with a significance of more than five standard deviations.

The European Physical Society Conference on High Energy Physics (EPS-HEP2025)
7-11 July 2025
Marseille, France

[1]For the CMS collaboration
[*]Speaker

PoS(EPS-HEP2025)285

1. Introduction

The Standard Model (SM) of particle physics successfully describes properties and interactions of elementary particles, but it cannot account for observed phenomena in the Universe, such as neutrino masses, dark matter, and the matter-antimatter asymmetry. It is possible to explore new physics scenarios by searching for discrepancies from the SM predictions in precise studies of SM observables and searches for very rare processes. In this context, the production of a single top quark in association with a WZ boson pair (tWZ) is particularly interesting as it offers enhanced sensitivity to the top quark's electroweak coupling (Figure 1). This very rare process is sensitive to unitarity-violating effects induced by modified electroweak interactions [1, 2], which can be interpreted in the Standard Model Effective Field Theory (SMEFT) framework [3, 4]. These proceedings present the first observation of the tWZ process [5], achieved by analysing 200 fb^{-1} of data collected by the CMS experiment. This dataset comprises 138 fb^{-1} recorded at $\sqrt{s} = 13\,\mathrm{TeV}$ [6], with the remainder collected at 13.6 TeV [7].

2. Simulation of signal and background

The tWZ final states exhibit many similarities with those of top quark pair production in association with a Z boson ($\mathrm{t\bar{t}Z}$), posing significant theoretical and experimental challenges for measuring tWZ. In particular, the modelling of the tWZ process requires special attention when simulated at next-to-leading order (NLO) in QCD, as contributions of the type $\mathrm{gg} \rightarrow \mathrm{tWZb}$ must be included. These diagrams can feature a resonant top quark pair causing overlap with the LO $\mathrm{t\bar{t}Z}$ process [2]. Therefore, the tWZ process is simulated using MadGraph5_aMC@NLO [8, 9] at NLO in QCD and the overlap is removed using the MadSTR plugin [10], which implements both diagram removal (DR) and diagram subtraction (DS) techniques [11, 12]. The signal samples are generated using the DR1 subtraction scheme, while the DR2 scheme is considered to evaluate the uncertainty in the signal modelling. Also the experimental identification of tWZ is very challenging due to its very small cross section, namely 136^{+9}_{-8} fb at $\sqrt{s} = 13\,\mathrm{TeV}$ and 148^{+10}_{-9} fb at 13.6 TeV at NLO in QCD [8, 9]. The main backgrounds are the $\mathrm{t\bar{t}Z}$ and tZq processes, which are simulated at

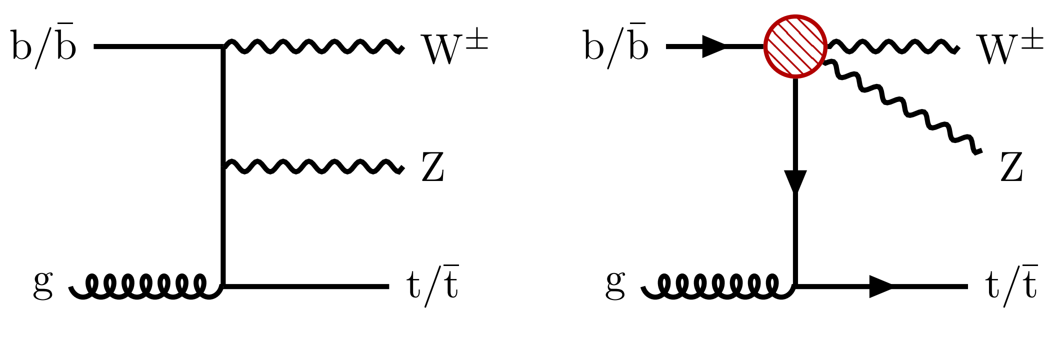

Figure 1: Example Feynman diagrams for tWZ production in the SM (left) and for anomalous tWZ production through an effective interaction (right). Figure from Ref. [5].

NLO accuracy in QCD using MadGraph5_aMC@NLO. The $t\bar{t}Z$ cross section is scaled to include approximate next-to-next-NLO (aN^{3}LO) QCD and NLO electroweak corrections [13]. The WZ process is simulated using POWHEG v2 [14–18]; while, smaller backgrounds are simulated using MadGraph5_aMC@NLO, POWHEG, and MCFM v7.0.1 [19, 20].

3. Analysis strategy

Events with three or four leptons and at least one b-tag jet are included in the signal regions (SRs) to enhance the sensitivity to tWZ. Electrons and muons are required to have $p_T > 10$ GeV and $p_T > 15$ GeV for events collected at $\sqrt{s} = 13$ and $\sqrt{s} = 13.6$ TeV, respectively. Electrons must have $|\eta| < 2.5$ and muons $|\eta| < 2.4$. Leptons are identified using multivariate analysis techniques, trained separately for 13 and 13.6 TeV data. The machine learning (ML) algorithms for 13 TeV data have efficiencies of 87 and 92% for electrons and muons, respectively. A tighter working point with efficiencies of 60 and 84% for electrons and muons, but with a threefold improvement in background rejection, is employed for 13.6 TeV data. Jets must have $p_T > 25$ GeV and $|\eta|<2.4$, and be separated from leptons by a $\Delta R > 0.4$. The b jets are selected using the DeepJet algorithm for 13 TeV data, while the ParticleTransformerAK4 algorithm is used for 13.6 TeV data, resulting in improved performance [21, 22]. The b-tag identification efficiencies are around 80%, with misidentification rates of about 1% for light jets and about 14% for charm quark jets.

Despite the tight physics object selection, the tWZ process accounts for only a small fraction of the event yields, due to the presence of several background processes with final states similar to tWZ but much larger cross sections. The leading background is $t\bar{t}Z$ followed by WZ, tZq, and processes with nonprompt leptons. Nonprompt leptons are defined as reconstructed leptons not originating from the decay of a W or a Z boson. Their contribution is estimated from data as it is often poorly modelled in simulation. Dedicated control regions (CRs) are defined to accurately model the nonprompt lepton contribution and constrain the normalization of the dominant backgrounds. Signal and control regions are identified based on the number of leptons, jets, b jets, p_T^{miss}, and the di-lepton invariant mass ($m_{\ell\ell}$) of the opposite-sign-same-flavor (OSSF) lepton pairs. The OSSF leptons are considered inside the mass window of the Z boson if their $m_{\ell\ell}$ is within 15 GeV from m_Z. The $SR_{3\ell}$ requires the presence of three leptons, at least two jets, one b jet, and an OSSF lepton pair inside the Z boson mass window. The $SR_{4\ell}$ requires the presence of four leptons, one b jet and exactly one OSSF lepton pair inside the Z boson mass window. In addition, four different CRs are also defined. Events with four leptons, two OSSF lepton pairs inside the Z boson mass window, and at least one jet are selected in the CR_{ZZ}. The CR_{WZ} includes events with three leptons, one OSSF lepton pair inside the Z boson mass window, at least two jets, zero b jet, $p_T^{miss} > 40$ GeV. This control region is also used to reweight the jet multiplicity distribution of WZ events in simulation to that measured in data, resulting in a significant improvement in the modelling of additional jet emissions. The jet multiplicity distribution measured in the CR_{WZ} is used as input to the maximum likelihood fit to constrain the associated uncertainty. Instead, the event yield distribution is used in the case of the CR_{ZZ}. The CR_{DY} is defined requiring the presence of three leptons, one OSSF lepton pair inside the Z boson mass window, zero b jet, and $p_T^{miss} < 40$ GeV. The $CR_{t\bar{t}}$ includes events with three leptons, at least two jets, one b jet, and no OSSF lepton pair inside the Z boson mass window. These two control regions are used to estimate nonprompt lepton contribution.

PoS(EPS-HEP2025)285

The contribution of the nonprompt lepton background is estimated from a fit to data simultaneously with the signal extraction. Dedicated nuisance parameters are constructed for the different nonprompt lepton categories and constrained in the fit using the trailing lepton p_T distribution measured in CR_{DY} and $CR_{t\bar{t}}$. The category indicates whether the nonprompt lepton originates from a b jet, a light jet, or a photon.
Dedicated machine learning algorithms based on the Particle Transformer (PᴀʀT) architecture [23] are trained to separate tWZ from the background. Different trainings are performed for 13 and 13.6 TeV data. The input variables include the four-momentum vector of leptons and jets in the events, as well as information about the missing transverse energy, b-tagging and particle ID. The output distributions of the ML algorithms are used as input to the maximum likelihood fit for the $SR_{3\ell}$ and $SR_{4\ell}$. The classifier used in the $SR_{3\ell}$ has four different output nodes targeting tWZ, $t\bar{t}Z$, WZ, and additional backgrounds. Three distributions are defined according to the node with the highest score: one enriched in tWZ events, one dominated by $t\bar{t}Z$ events to constrain its normalization, and one containing events classified as WZ or other backgrounds to constrain the associated uncertainties. Because of the limited statistical precision, a binary classifier is employed for the $SR_{4\ell}$ and its output is included as an input to the fit. Figure 2 shows the tWZ and $t\bar{t}Z$ output node distributions in the $SR_{3\ell}$, along with the ML output distribution obtained in the $SR_{4\ell}$.

4. Systematic uncertainties

The systematic uncertainties are treated as nuisance parameters in the maximum likelihood fit used to extract the signal strength of the tWZ process. Several sources of systematic uncertainties are considered, including theoretical and experimental uncertainties. The experimental uncertainties include those on the pileup description, jet energy corrections and resolution, trigger efficiency, lepton efficiency, and b-tagging corrections. The integrated luminosity has an uncertainty of 1.6% for the 2016–2018 data-taking years, and 1.4 and 1.3% for 2022 and 2023, respectively. Unconstrained nuisance parameters are used to describe the contribution of nonprompt leptons from jets, while nuisances with Gaussian priors are used for nonprompt leptons coming from photons. The theoretical uncertainties include those on the parton distribution functions, parton shower simulation, and matrix element renormalization and factorization scales. The differences between the DR1 and DR2 subtraction schemes are taken into account as signal modelling uncertainty. Variations from DS are not considered, as these are smaller than the ones derived with DR2. A shape uncertainty is assigned to the jet multiplicity reweighting for the WZ process by considering two alternative configurations: one where the correction factor is doubled and another where no correction is applied. In addition, theoretical uncertainties in the cross sections of the background processes are considered. A normalization uncertainty of 7% is used for the $t\bar{t}Z$ cross section [24, 25]. Two distinct normalization uncertainties are employed for the WZ and ZZ processes, a 20% uncertainty is assigned to VV+b production [26] and a 10% uncertainty to VV+j [27]. An uncertainty of 11% is employed for tZq production [26], and a 10% uncertainty for multi-boson processes [28, 29] and photon associated production modes [30]. Uncertainties of 5 and 10% are assigned to the $t\bar{t}$ [31] and DY processes [32]. A 25% uncertainty is used for the $t\bar{t}W$ process to account for the discrepancy between measurements and SM predictions [33], and a 20% uncertainty is used for $t(\bar{t})X$ [34–36], which includes minor backgrounds from single top and top quark pair

PoS(EPS-HEP2025)285

associated productions. Finally, uncertainties arising from the finite size of simulated samples are included using the Barlow–Beeston light method [37].

5. Results

The signal strength of tWZ is measured to be $\mu_{\mathrm{tWZ}} = 1.77 \pm 0.32$, with an observed statistical significance of 5.8 s.d. compared to the background-only hypothesis, with 3.5 s.d. expected. This result constitutes the first observation of the tWZ process and agrees within 2.3 s.d. with the SM predictions. The measured cross sections are 248 ± 52 fb and 242 ± 77 fb for $\sqrt{s}$ = 13 and

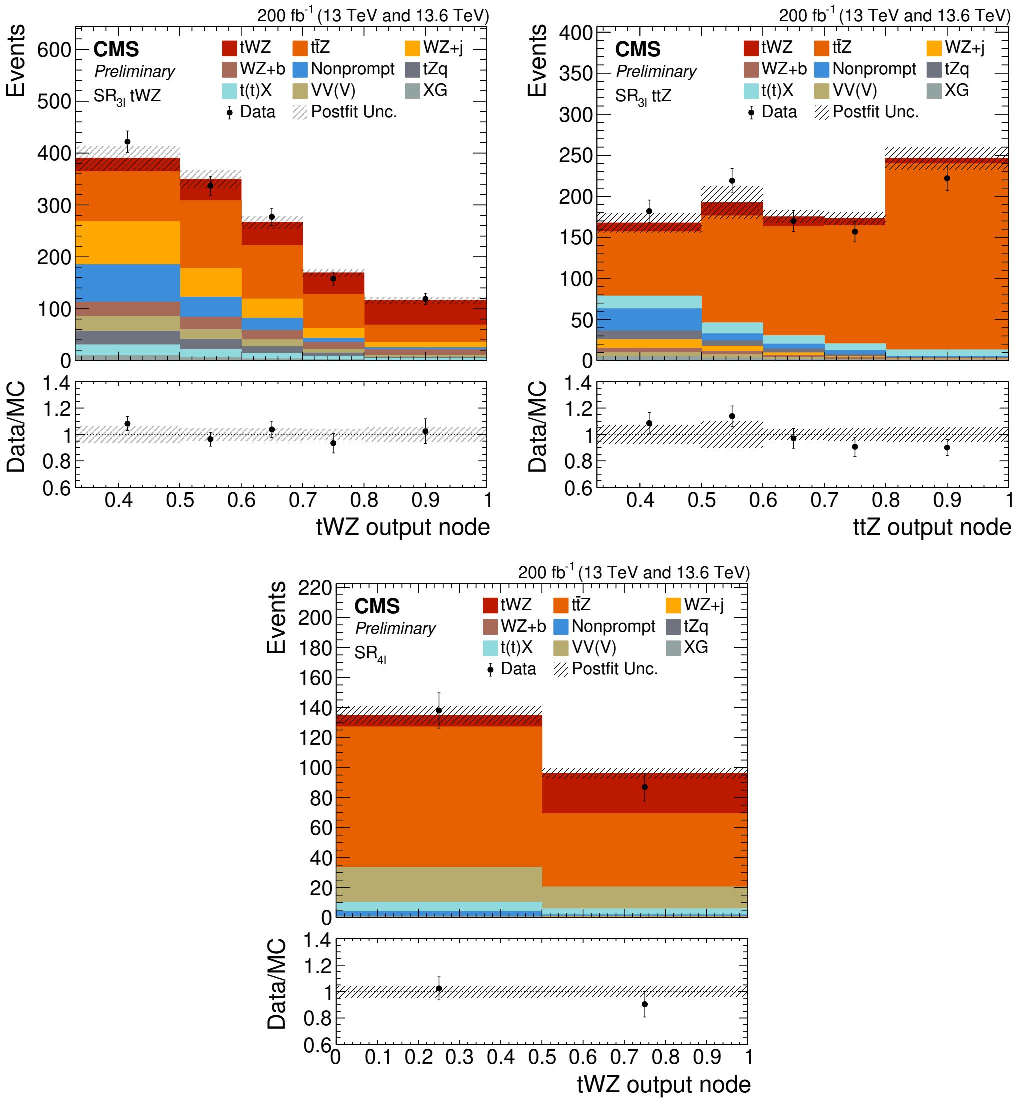

Figure 2: Distributions in the classifier output nodes for the tWZ (upper left) and $t\bar{t}Z$ (upper right) nodes in $SR_{3\ell}$, and in the classifier output node in $SR_{4\ell}$ (lower) after a fit to the data. The dashed band shows the postfit uncertainty. The ratio of data to the predictions from MC simulation is shown below the distributions. Figure from Ref. [5].

13.6 TeV, respectively. The dominant uncertainties are the normalization uncertainties of the $t\bar{t}Z$ and WZ + b jet backgrounds. The correlation between tWZ and $t\bar{t}Z$ is studied in a dedicated fit where the $t\bar{t}Z$ normalization is left unconstrained (Figure 3). The measured signal strengths are $\mu_{tWZ} = 1.88 \pm 0.34$ and $\mu_{t\bar{t}Z} = 0.91 \pm 0.05$, also resulting in a significance of more than 5 s.d. for tWZ production. The signal strength of the $t\bar{t}Z$ process is compatible within 2 s.d. with the most recent theoretical prediction at aN^3LO QCD and NLO EW [13].

This result represents a significant improvement with respect to the previous analysis [38], both in terms of reduced correlation between tWZ and $t\bar{t}Z$ and improved tWZ sensitivity. In particular, the expected significance increases from 1.4 s.d. to 3.0 s.d., when considering the same dataset. The observation of the tWZ process [5] marks a significant step forward in our understanding of the top quark-electroweak interaction. Higher statistical precision is needed to enable SMEFT interpretations of the tWZ process through future differential results to interpret the observed excess.

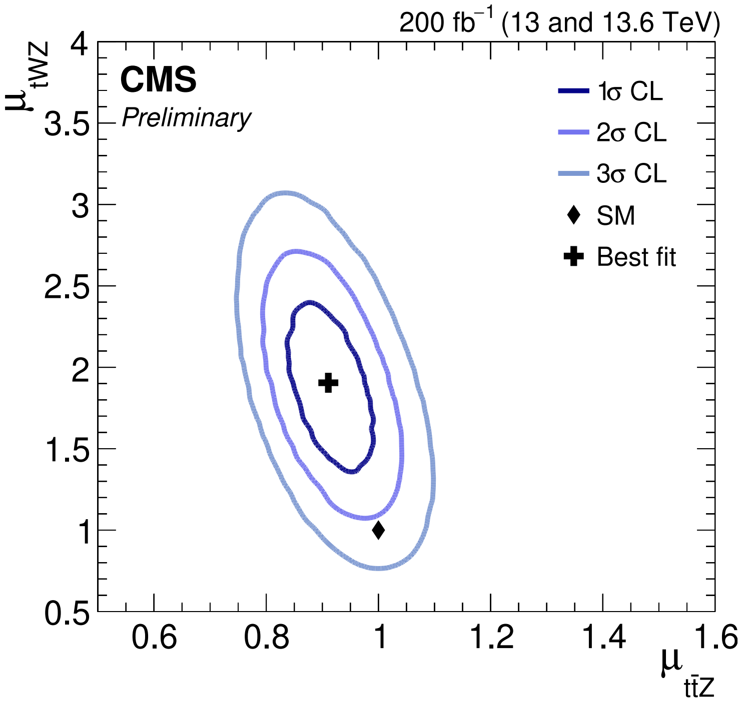

Figure 3: Likelihood scan of the signal strengths for tWZ and $t\bar{t}Z$ production. The contours in different shades of blue correspond to the 68%, 95%, and 99% confidence level. The black diamond indicates the SM expected value, while the black cross shows the best fit value. Figures from Ref. [5].

References

[1] F. Maltoni, L. Mantani, and K. Mimasu, "Top-quark electroweak interactions at high energy", *JHEP* **10** (2019) 004, doi:10.1007/JHEP10(2019)004, arXiv:1904.05637.

[2] H. E. Faham, F. Maltoni, K. Mimasu, and M. Zaro, "Single top production in association with a WZ pair at the LHC in the SMEFT", *JHEP* **01** (2022) 100, doi:10.1007/JHEP01(2022)100, arXiv:2111.03080.

[3] J. Keaveney, "Constraining the SMEFT with a differential cross section measurement of tWZ production at the HL-LHC", *Phys. Rev. D* **107** (2023), no. 3, 036021, doi:10.1103/PhysRevD.107.036021, arXiv:2107.01053.

[4] A. Belvedere, C. Englert, R. Kogler, and M. Spannowsky, "Dispelling the $\sqrt{\mathcal{L}}$ myth for the High-Luminosity LHC", *Eur. Phys. J. C* **84** (2024), no. 7, 715, doi:10.1140/epjc/s10052-024-13032-w, arXiv:2402.07985.

[5] CMS Collaboration, "Observation of tWZ production at the CMS experiment". CMS-PAS-TOP-24-009, 2025.

[6] CMS Collaboration, "The CMS Experiment at the CERN LHC", *JINST* **3** (2008) S08004, doi:10.1088/1748-0221/3/08/S08004.

[7] CMS Collaboration, "Development of the CMS detector for the CERN LHC Run 3", *JINST* **19** (2024), no. 05, P05064, doi:10.1088/1748-0221/19/05/P05064, arXiv:2309.05466.

[8] J. Alwall et al., "The automated computation of tree-level and next-to-leading order differential cross sections, and their matching to parton shower simulations", *JHEP* **07** (2014) 079, doi:10.1007/JHEP07(2014)079, arXiv:1405.0301.

[9] R. Frederix and S. Frixione, "Merging meets matching in MC@NLO", *JHEP* **12** (2012) 061, doi:10.1007/JHEP12(2012)061, arXiv:1209.6215.

[10] S. Frixione et al., "Automated simulations beyond the Standard Model: supersymmetry", *JHEP* **12** (2019) 008, doi:10.1007/JHEP12(2019)008, arXiv:1907.04898.

[11] S. Frixione et al., "Single-top hadroproduction in association with a W boson", *JHEP* **07** (2008) 029, doi:10.1088/1126-6708/2008/07/029, arXiv:0805.3067.

[12] C. D. White, S. Frixione, E. Laenen, and F. Maltoni, "Isolating Wt production at the LHC", *JHEP* **11** (2009) 074, doi:10.1088/1126-6708/2009/11/074, arXiv:0908.0631.

[13] N. Kidonakis and C. Foster, "Higher-order soft-gluon corrections for $t\bar{t}Z$ cross sections", *Phys. Lett. B* **860** (2025) 139146, doi:10.1016/j.physletb.2024.139146, arXiv:2410.01214.

PoS(EPS-HEP2025)285

[14] P. Nason, "A New method for combining NLO QCD with shower Monte Carlo algorithms", *JHEP* **11** (2004) 040, doi:10.1088/1126-6708/2004/11/040, arXiv:hep-ph/0409146.

[15] S. Frixione, P. Nason, and C. Oleari, "Matching NLO QCD computations with Parton Shower simulations: the POWHEG method", *JHEP* **11** (2007) 070, doi:10.1088/1126-6708/2007/11/070, arXiv:0709.2092.

[16] S. Frixione, P. Nason, and G. Ridolfi, "A Positive-weight next-to-leading-order Monte Carlo for heavy flavour hadroproduction", *JHEP* **09** (2007) 126, doi:10.1088/1126-6708/2007/09/126, arXiv:0707.3088.

[17] S. Alioli, P. Nason, C. Oleari, and E. Re, "A general framework for implementing NLO calculations in shower Monte Carlo programs: the POWHEG BOX", *JHEP* **06** (2010) 043, doi:10.1007/JHEP06(2010)043, arXiv:1002.2581.

[18] E. Re, "Single-top Wt-channel production matched with parton showers using the POWHEG method", *Eur. Phys. J. C* **71** (2011) 1547, doi:10.1140/epjc/s10052-011-1547-z, arXiv:1009.2450.

[19] J. M. Campbell, R. K. Ellis, and C. Williams, "Vector Boson Pair Production at the LHC", *JHEP* **07** (2011) 018, doi:10.1007/JHEP07(2011)018, arXiv:1105.0020.

[20] J. M. Campbell, R. K. Ellis, and W. T. Giele, "A Multi-Threaded Version of MCFM", *Eur. Phys. J. C* **75** (2015), no. 6, 246, doi:10.1140/epjc/s10052-015-3461-2, arXiv:1503.06182.

[21] CMS Collaboration, "Run 3 commissioning results of heavy-flavor jet tagging at $\sqrt{s}$ = 13.6 TeV with CMS data using a modern framework for data processing". CMS-DP-2022-024, 2024.

[22] CMS Collaboration, "Performance summary of AK4 jet b tagging with data from 2022 proton-proton collisions at 13.6 TeV with the CMS detector". CMS-DP-2022-025, 2024.

[23] H. Qu, C. Li, and S. Qian, "Particle Transformer for Jet Tagging", arXiv:2202.03772.

[24] CMS Collaboration, "Measurements of inclusive and differential cross sections for top quark production in association with a Z boson in proton-proton collisions at $\sqrt{s}$ = 13 TeV", *JHEP* **02** (2025) 177, doi:10.1007/JHEP02(2025)177, arXiv:2410.23475.

[25] ATLAS Collaboration, "Inclusive and differential cross-section measurements of $t\bar{t}Z$ production in pp collisions at $\sqrt{s}$ = 13 TeV with the ATLAS detector, including EFT and spin-correlation interpretations", *JHEP* **07** (2024) 163, doi:10.1007/JHEP07(2024)163, arXiv:2312.04450.

[26] CMS Collaboration, "Inclusive and differential cross section measurements of single top quark production in association with a Z boson in proton-proton collisions at $\sqrt{s}$ = 13 TeV", *JHEP* **02** (2022) 107, doi:10.1007/JHEP02(2022)107, arXiv:2111.02860.

[27] CMS Collaboration, "Measurement of the inclusive and differential WZ production cross sections, polarization angles, and triple gauge couplings in pp collisions at $\sqrt{s} = 13$ TeV", *JHEP* **07** (2022) 032, doi:10.1007/JHEP07(2022)032, arXiv:2110.11231.

[28] CMS Collaboration, "Observation of the production of three massive gauge bosons at $\sqrt{s} = 13$ TeV", *Phys. Rev. Lett.* **125** (2020) 151802, doi:10.1103/PhysRevLett.125.151802, arXiv:2006.11191.

[29] ATLAS Collaboration, "Observation of $W\gamma\gamma$ triboson production in proton-proton collisions at $\sqrt{s} = 13$ TeV with the ATLAS detector", *Phys. Lett. B* **848** (2024) 138400, doi:10.1016/j.physletb.2023.138400, arXiv:2308.03041.

[30] CMS Collaboration, "Observation of $WW\gamma$ production and search for $H\gamma$ production in proton-proton collisions at $\sqrt{s} = 13$ TeV", *Phys. Rev. Lett.* **132** (2024) 121901, doi:10.1103/PhysRevLett.132.121901, arXiv:2310.05164.

[31] M. Czakon and A. Mitov, "Top++: A Program for the Calculation of the Top-Pair Cross-Section at Hadron Colliders", *Comput. Phys. Commun.* **185** (2014) 2930, doi:10.1016/j.cpc.2014.06.021, arXiv:1112.5675.

[32] CMS Collaboration, "Measurement of differential cross sections for the production of a Z boson in association with jets in proton-proton collisions at $\sqrt{s} = 13$ TeV", *Phys. Rev. D* **108** (2023) 052004, doi:10.1103/PhysRevD.108.052004, arXiv:2205.02872.

[33] CMS Collaboration, "Measurement of the cross section of top quark-antiquark pair production in association with a W boson in proton-proton collisions at $\sqrt{s} = 13$ TeV", *JHEP* **07** (2023) 219, doi:10.1007/JHEP07(2023)219, arXiv:2208.06485.

[34] CMS Collaboration, "Measurement of inclusive and differential cross sections for single top quark production in association with a W boson in proton-proton collisions at $\sqrt{s} = 13$ TeV", *JHEP* **07** (2023) 046, doi:10.1007/JHEP07(2023)046, arXiv:2208.00924.

[35] CMS Collaboration, "A portrait of the Higgs boson by the CMS experiment ten years after the discovery.", *Nature* **607** (2022), no. 7917, 60–68, doi:10.1038/s41586-022-04892-x, arXiv:2207.00043. [Erratum: Nature 623, (2023)].

[36] CMS Collaboration, "Observation of four top quark production in proton-proton collisions at s=13TeV", *Phys. Lett. B* **847** (2023) 138290, doi:10.1016/j.physletb.2023.138290, arXiv:2305.13439.

[37] R. J. Barlow and C. Beeston, "Fitting using finite Monte Carlo samples", *Comput. Phys. Commun.* **77** (1993) 219–228, doi:10.1016/0010-4655(93)90005-W.

[38] CMS Collaboration, "Evidence for tWZ production in proton-proton collisions at $\sqrt{s} = 13$ TeV in multilepton final states", *Phys. Lett. B* **855** (2024) 138815, doi:10.1016/j.physletb.2024.138815, arXiv:2312.11668.